Cross-limb communication during *Xenopus* hindlimb regenerative response: non-local bioelectric injury signals

Sera M. Busse[1,2], Patrick T. McMillen[1,2] and Michael Levin[1,2,*]

ABSTRACT

Regeneration of damaged body parts requires coordination of size, shape, location and orientation of tissue with the rest of the body. It is not currently known to what extent injury sites communicate with the remaining soma during repair, or what information may emanate from the injury site and reach other regions. We examined the bioelectric properties (resting potential gradients in the epidermis) of *Xenopus laevis* froglets undergoing hindlimb amputation and observed that the contralateral (undamaged) limb exhibits apparent depolarization signals immediately after the opposite hindlimb is amputated. The pattern of depolarization matches that of the amputated limb and is correlated to the position and type of injury, revealing that information about damage is available to remote body tissues and is detectable non-invasively *in vivo* by monitoring the bioelectric state. These data extend knowledge about the electrophysiology of regenerative response, identify a novel communication process via long-range spread of injury signaling, a phenomenon that we call bioelectric injury mirroring, and suggest revisions both to regenerative medicine and diagnostic strategies that are focused entirely on the wound site, and to the use of contralateral limbs as controls.

KEY WORDS: Frog, Regeneration, Bioelectrics, Resting potential, Long-range signaling

INTRODUCTION

Many organisms, including axolotls and planaria, are able to regenerate nearly all of the tissues and organ structures in their bodies (Nacu et al., 2016; Tanaka, 2016; Tanaka and Reddien, 2011). In contrast, humans exhibit limited regenerative capacity, largely restricted to the intestinal lining, liver and blood, and cannot regenerate full limbs (Poss, 2010). In order to augment an animal's innate regenerative ability, it is important to understand the flow of patterning information to and from the sites of injury and rebuilding. For example, the two fragments of a bisected planarian must regenerate a head and tail, respectively, even though the cells at the wound sites were adjacent before the cut. They shared the same positional information, and yet grow into opposing anatomical structures, revealing the importance of communication between the wound site and the rest of the body. Other examples of large-scale remodeling in vertebrates underscore the importance of non-local information for regenerative pattern homeostasis. Although it is clear that regeneration must rebuild structures that are properly matched to the host body in terms of size, shape and orientation, it is not yet known to what extent and what kind of information might be exchanged to and from a wound site.

Recent work has shown striking systemic biochemical responses to amputation in axolotl limbs (Johnson et al., 2017). Classic examples of long-range responses to injury in mammals include phenotypes in contralateral deer antlers (Bubenik and Pavlansky, 1965; Bubenik, 1990; Marburger et al., 1972), whereas recent studies have begun to reveal body-wide chemical factors that regulate stem cell activity after injury (Rodgers et al., 2017). Here, we focused on bioelectrical properties: resting potential gradients (V_{mem}) across non-neural tissues, which have previously been implicated in numerous regenerative events across phyla (Borgens, 1986; Frazee, 1909; Levin, 2007, 2014a,b; Levin et al., 2017; Morgan and Dimon, 1904; Rose, 1974; Smith, 1974; Tseng and Levin, 2013). We asked whether specific information about an amputation injury might be available at distant locations in the vertebrate body, and whether it could be detected (and analyzed) by monitoring the bioelectric state of organs that are a considerable distance from a significant injury site.

Spatial gradients of bioelectric state are known to regulate a wide range of cell behaviors (Bates, 2015; Funk, 2013; Levin and Martyniuk, 2017; McCaig et al., 2005; Wang and Zhao, 2010), such as proliferation and differentiation in both stem cells (Sundelacruz et al., 2009; Yasuda and Adams, 2010) and somatic cells (Adams et al., 2016; Durant et al., 2017; Levin et al., 2002; Perathoner et al., 2014; Vandenberg et al., 2011) during growth and patterning. The recent development of imaging methods for resting potential *in vivo* (Adams and Levin, 2012a,b; Oviedo et al., 2008) facilitates the monitoring of endogenous bioelectric signaling processes and their readouts. This somatic bioelectric system is an evolutionary precursor to, and operates in tandem with, the more familiar neural controls (Borodinsky and Belgacem, 2016; Borodinsky et al., 2012; Herrera-Rincon et al., 2017; Swapna and Borodinsky, 2012).

Xenopus laevis can regenerate their hindlimbs for a period of time following metamorphosis, after which this ability is lost (Dent, 1962; Slack et al., 2004, 2008; Tseng and Levin, 2008). Classic data has implicated bioelectric parameters as being indicative of regeneration response (Borgens et al., 1977a,b; Sharma and Niazi, 1990; Smith, 1974); more recent work in this field has focused on the use of molecular techniques for regulating regenerative bioelectrics. In non-regenerative-stage animals, tail regeneration can be rescued by inducing a bioelectric state that is seen in younger-stage froglets via genetically targeting ion pumps (Adams et al., 2007), pharmacologically regulating sodium channels (Tseng et al., 2010) or even with optogenetics (Adams et al., 2013).

Previous work on regeneration in *Xenopus* has largely focused on the wound region and the activity of cells therein (Golding et al., 2016; King et al., 2012; Lin et al., 2013; Neff et al., 2011; Yokoyama et al., 2011a,b). Interestingly, bioelectric signals also function at longer ranges. Modifying V_{mem} in cells on the opposite

[1]Biology Department and Allen Discovery Center, Tufts University, Medford, MA 02155, USA. [2]Wyss Institute for Biologically Inspired Engineering at Harvard University, Boston, MA 02115, USA.

*Author for correspondence (michael.levin@tufts.edu)

M.L., 0000-0001-7292-8084

side of a tadpole regulates the incidence of tumorigenesis from oncogene mis-expression (Chernet et al., 2015; Chernet and Levin, 2014), the bioelectric state of ventral cells helps shape proliferation and apoptosis in the nascent brain (Pai et al., 2015a,b), and cells in both frog and chick embryos need to communicate with the opposite side of the animal via physiological gradients to acquire the correct laterality (Levin and Mercola, 1999).

Given the importance of bioelectric states in regeneration-relevant events, we investigated the possibility that information about injury might be detected in distant regions by examining their resting potential profiles. We established a leg amputation and bioelectric imaging assay, which uncovered a remarkable and previously unknown phenomenon, which we call bioelectric injury mirroring (BIM). A contralateral uninjured leg reveals bioelectric states that provide information about the location and type of injury occurring on the opposite side.

RESULTS

Depolarization in contralateral limb occurs in response to amputation

To examine the responses to injury in distant tissue, we performed amputations of one limb and examined the bioelectric state in the other (contralateral) limb of each animal. The right hindlimbs of regenerative-stage frogs (stages 51-55) (Nieuwkoop and Faber, 1967) were amputated (see Materials and Methods for details); after soaking in $DiBAC_4(3)$ for 30 min, the hindlimbs were individually imaged and the fluorescent signals were analyzed with ImageJ software to determine the location and size of any areas of depolarization of the surface layer of cells in the uninjured leg. Individual cell types cannot definitively be identified in this experiment, because molecular markers require fixation and voltage gradients do not persist in dead cells. Dye imaging can only detect a signal from the top layer of cells (because of the opacity of frog skin), so this strongly suggests that the tissue involved is the epidermis (Fig. S1A). Remarkably, we observed that, after amputation, froglets began to exhibit depolarization in their unamputated contralateral limbs (Fig. 1A,B), although in a minority (8 out of 42) of amputated froglets we detected a signal less than or equal to that of the average basal signal seen in control animals. We observed that most of the contralateral limbs became depolarized by 1 h post amputation (HPA) and showed significantly more $DiBAC_4(3)$ signal than was seen in the limbs of control (unamputated) froglets of the same stage ($P<0.0001$) (Fig. 1C, Fig. S1B).

We verified that $DiBAC_4(3)$ imaging reveals depolarization events in limbs, as has previously been reported for other tissues in frog and other model species (Adams and Levin, 2012b; Adams et al., 2016; Jang et al., 2011; Krotz et al., 2004; Oviedo et al., 2008; Pai et al., 2015a; Pare et al., 2017; Vandenberg et al., 2011; Wolff et al., 2003). We soaked froglets in 90 mM potassium gluconate, which decreases the gradient of K^+ ions across the membrane that separates extracellular solution and the inside of the cells. This reduces the normal efflux of potassium out of cells via K^+ channels, thereby causing a less hyperpolarized V_{mem}, which should be detected via a brighter $DiBAC_4(3)$ signal. As an additional control, we soaked a separate group of froglets in a solution of 90 mM KCl, using the high extracellular chloride (which can enter cells via Cl^- channels and pumps) to counteract the depolarizing effect of the potassium ions. As predicted, upon treatment froglets soaked in the potassium gluconate solution showed a significantly increased $DiBAC_4(3)$ signal ($P<0.01$) compared with both control and KCl-treated froglets, which indicated that a key

determinant of the fluorescent dye signal is the ionic state of the tissue (Fig. S2A,B).

We further sought to confirm that a depolarization signal in response to potassium gluconate treatment is not specific to only amputated limbs, and to demonstrate the ability of $DiBAC_4(3)$ to report distinct levels of depolarization that match differential extracellular levels of potassium. We incubated uncut froglets in increasing concentrations of potassium gluconate and, as predicted, we observed a stepwise increase in signal (Fig. S2C). As a result of these control experiments, and in light of the extensive literature implicating $DiBAC_4(3)$ as a sensor for depolarized cells (Adams and Levin, 2012a,b; Adams et al., 2007, 2016; Beane et al., 2011, 2013; Blackiston et al., 2011; Chernet and Levin, 2013; Ivanov et al., 2013; Jang et al., 2011; Jia et al., 2013; Oviedo et al., 2008; Pai et al., 2012; Vandenberg et al., 2011; Wolff et al., 2003), we will refer to $DiBAC_4(3)^+$ cells as depolarized in this paper, though additional factors that can contribute to this signal are described in the Discussion section.

Depolarization occurs quickly in the contralateral limb

After investigating the V_{mem} changes that occur in regenerative-stage froglets over a 48 h time period, we determined that tadpole hindlimbs are depolarized by 0.5 HPA, but became markedly less depolarized by 24 HPA ($P<0.0001$). There was no further significant decrease in depolarization from 24 to 48 HPA (Fig. 2A,B). We then sought to determine how quickly the contralateral limb received information indicating that the opposing limb had been amputated. Froglets at stage 53 (regenerative) were pre-emptively soaked in $DiBAC_4(3)$ and MS222 for 30 min before amputation, to allow the dye to permeate into the cells before amputation. The animals were then amputated and immediately imaged (Fig. 2C). Within 5 s of amputation, some depolarization of cells was observed in the contralateral limb. The signal continued to grow in strength until 0.5 HPA, which indicated that the one hour allotted between amputation and imaging in previous experiments was sufficient to allow depolarization to occur, and that, in fact, the depolarization signal in the unamputated limb is triggered within seconds of amputation.

Contralateral voltage signal reflects the position of the limb injury

We then investigated whether the contralateral leg can sense more than the mere presence of injury and how much information might be available to it, by asking whether the spatial pattern of depolarization reflected knowledge of the position of the cut in the amputated limb. By imaging voltage maps in amputated froglets, we recorded position data on the depolarization zones in the cut and contralateral limbs. In the cut limb we measured from the hip to the end of the stump, from the hip to the end of depolarization, from the hip to the mid-point of depolarization and from the hip to the start-point of depolarization. In the contralateral limb we measured from the hip to the start-point of depolarization, from the hip to the mid-point of depolarization, from the hip to the end-point of depolarization and from the end of the foot to the end of depolarization (Fig. S3A).

Regression analyses among these measurements showed specific regions of high correlation. There was a high correlation between the length of the amputated leg's stump and the length to the end-point of depolarization in the contralateral limb ($r=0.697$, $P<0.0001$) (Fig. 3A). There was a high correlation between the end-point of depolarization in both cut and contralateral limbs ($r=0.674$, $P<0.0001$) (Fig. S3B). The longer the length of the stump at
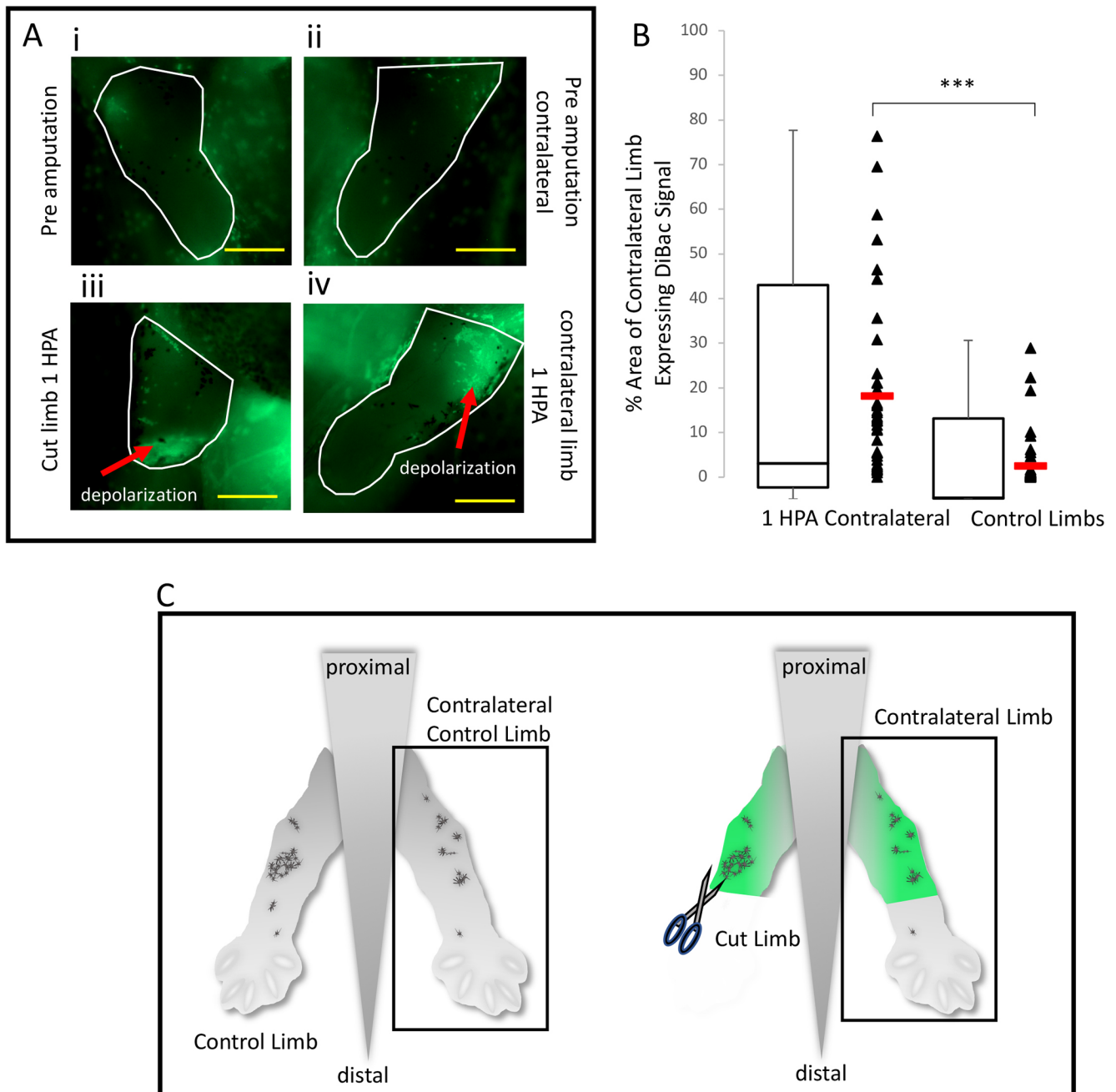
2

Fig. 1. Contralateral limbs respond to amputation of the opposite side. (A) Fluorescent imaging of amputated limb and non-amputated contralateral limb both pre-amputation (i,ii) and post-amputation (iii,iv) showing areas of depolarization of the surface layer of cells [DiBAC4(3) staining]. After amputation, froglets began to exhibit depolarization in their unamputated contralateral limbs. White outline indicates the boundaries of the limb. (B) Amputated froglets exhibited a significantly greater area of depolarization on contralateral uncut limbs than non-amputated froglets (two-tailed t-test; control, $n=57$; amputated, $n=42$; ***$P<0.0001$). The box and whisker plot represents the data to the right of it in a different form. The red horizontal lines are the means of each dataset. (C) Schematic indicating experimental procedure. Experiment replicated three times. Scale bars: 500 μm.

amputation, the further down the contralateral limb its depolarization signal stretched. We conclude that, as the contralateral limb's signal is correlated with the position of the cut, the information signal must bear information about the proximo-distal location of the injury, and that the contralateral leg acts on this information by performing its depolarization accordingly (Fig. 3B).

The midline of the froglet (yellow arrow, Fig. 3B) exhibited DiBAC$_4$(3) signal as well, but this standing pattern was observed in intact animals regardless of amputation and did not change in

response to leg injury. We did not observe changes in signal intensity in any other regions of the froglet following amputation (Fig. 3C).

Contralateral depolarization occurs in response to amputation but not injury

The opposite leg detects the presence and location of amputation, but does it receive any information about the type of injury? To determine whether the contralateral V_{mem} changes observed after amputation were a result of the general injury incurred by the
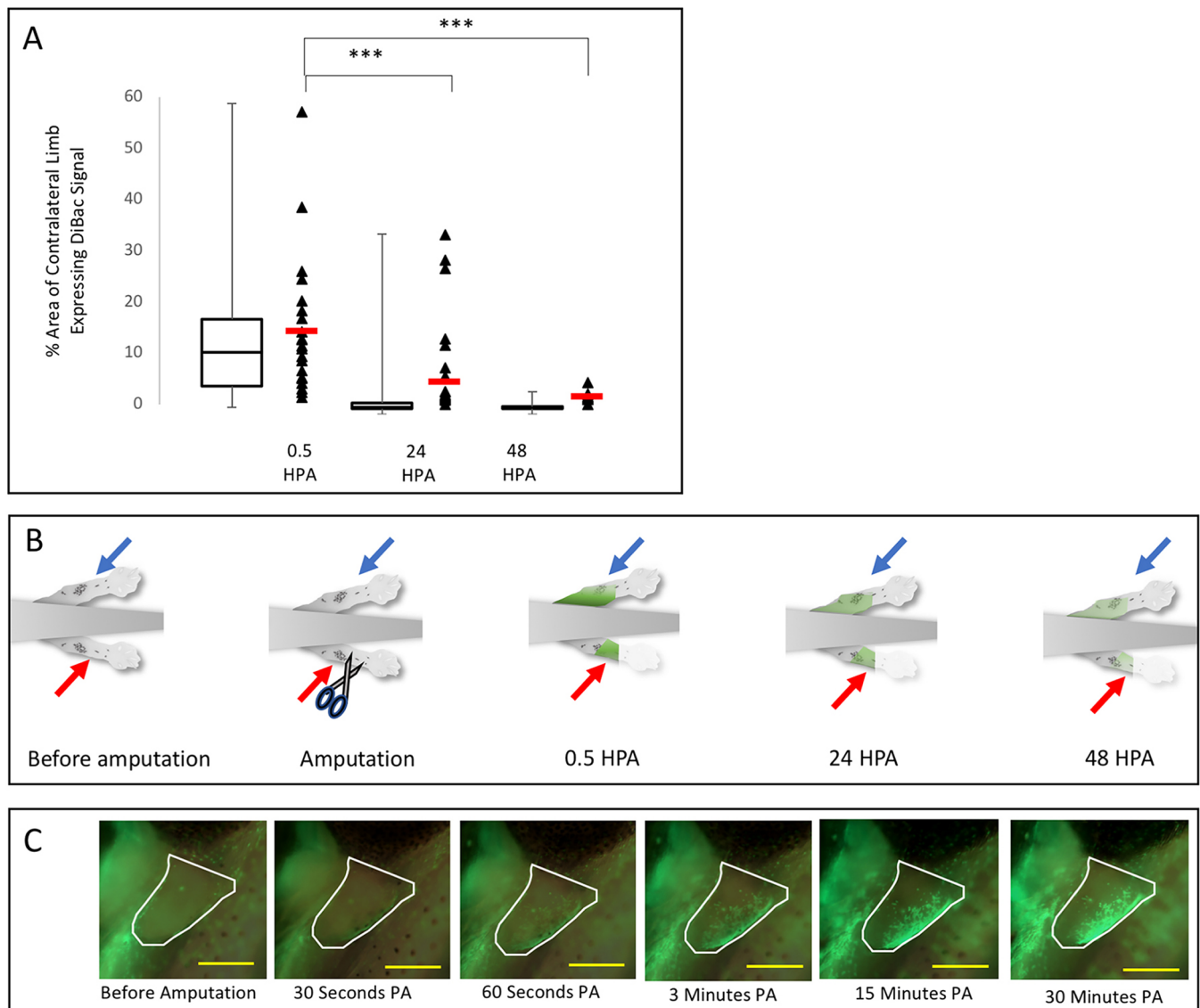
Fig. 2. The amputation 'signal' travels quickly to the contralateral limb and dissipates within 24 HPA. (A) To characterize the temporal nature of the amputation signal received by the contralateral limb, multiple imaging time points were observed following amputation. Froglets were amputated, and then imaged at 0.5 HPA, 24 HPA and 48 HPA. Signal area significantly decreased from 0.5 HPA to 24 HPA (Kruskal–Wallis test; 0.5 HPA, $n=23$; 24 HPA, $n=36$; 48 HPA, $n=20$; ***$P<0.0001$), but did not significantly decrease from 24 HPA to 48 HPA, suggesting that the signal causing depolarization peaks quickly and dissipates completely by 48 HPA. The experiment was replicated three times. (B) Schematic of the timeline of the experiment showing what changes occur at each time point/step. Red arrow, amputated limb; blue arrow, contralateral limb. (C) Time-lapse fluorescent imaging of the 30 min immediately following amputation [DiBAC4(3) staining], taken to determine how quickly the amputation signal reaches the contralateral limb. The signal first began to appear within 30 s following amputation and continued to grow in strength over the next 30 min. The experiment was replicated five times, and each replication showed this same trend. Scale bars: 500 µm.

tadpole or whether the response was specific to amputation, regenerative-stage froglets were randomly assigned one of two treatments: major injury or amputation (Fig. 4A). Those receiving the major injury treatment were punctured in the tibiofibular region of the right hindlimb with a syringe needle, which was then agitated to induce localized trauma without removing the limb. Animals receiving the amputation treatment were bisected at the tibiofibular region with small scissors. Whereas both injured and amputated froglets displayed significant levels of depolarization around the cut or injury site, the contralateral limbs of injured froglets were significantly less depolarized than the contralateral limbs of those animals subjected to amputation ($P<0.0001$, Fig. 4B,C). In fact, contralateral limbs of injured froglets exhibited only basal levels of depolarization, comparable with that seen in control limbs (Fig. 1B).

These results indicate that the depolarization signal observed after amputation is amputation-specific, whereas the depolarization observed at the site of amputation or injury appears to be a more general response to injury. Furthermore, these data reveal that depolarization of the injured limb does not directly induce depolarization of the contralateral limb.

Contralateral communication is limb-specific

To determine whether long-range bioelectric signaling likewise occurred in the contralateral counterparts of other organs within the froglets, one kidney or one eye of *Xenopus* embryos was removed and imaged with DiBAC$_4$(3). Embryo stages 37 and 24 were selected because, at those time points, respectively, kidneys and eyes exhibit regenerative capacities similar to those
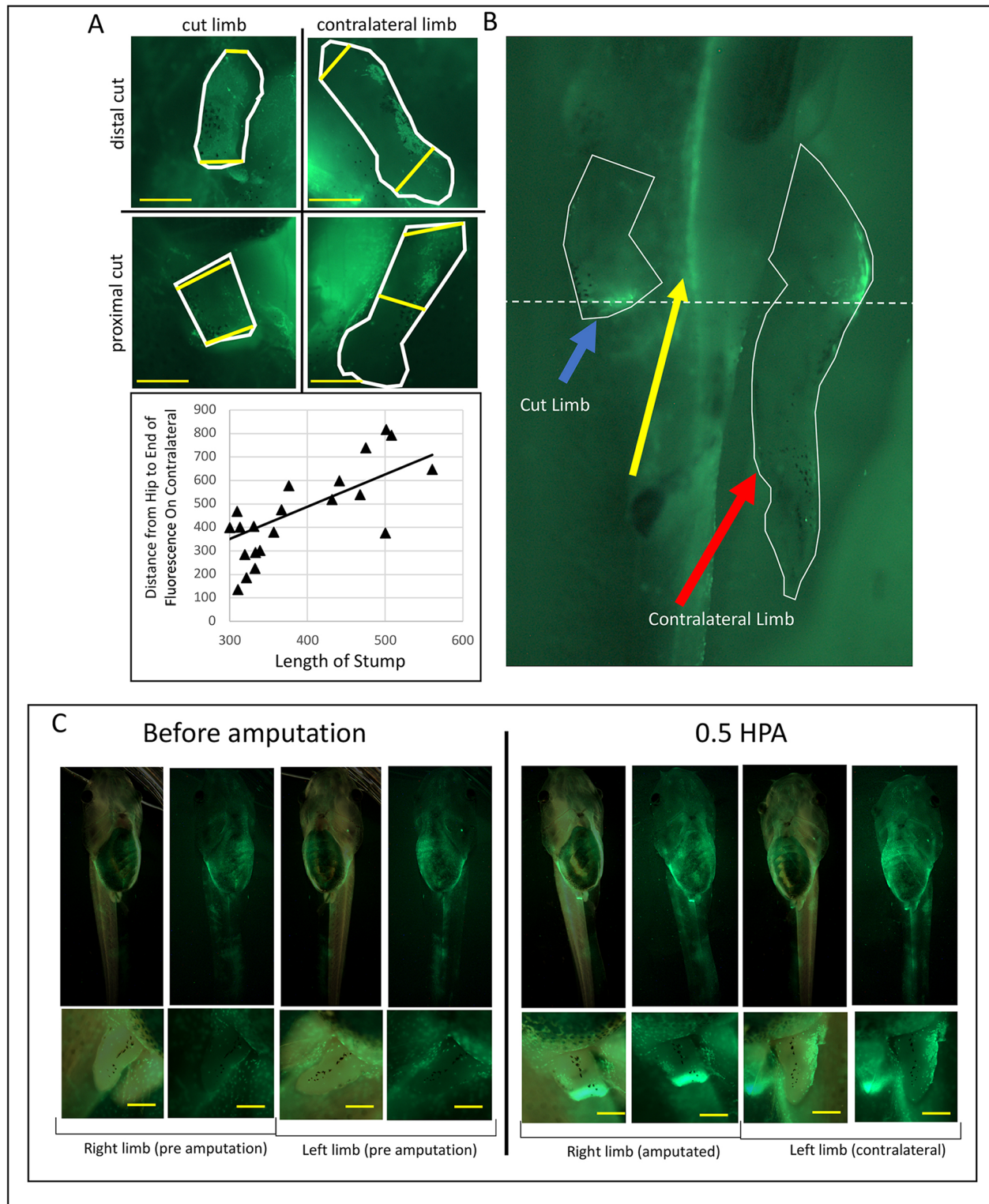
Fig. 3. Spatial information about the cut limb is exhibited on the contralateral limb. (A) Fluorescent imaging of amputated limb and non-amputated contralateral limb [DiBAC4(3) staining] (top panel) and quantification showing a significant correlation between the length of the stump left after amputation and the length that the $DiBAC_4(3)$ (depolarization) signal extended down the contralateral limb (bottom panel) (linear regression test; n=21; P<0.0001). The experiment was replicated three times. White outlines indicate the boundaries of the limb. Bold yellow lines indicate the start and finish points of the signal seen on each limb; the measurements were taken as described in the Results. (B) A 'midline signal' was often observed in bodies of both amputated and unamputated frogs (yellow arrow). This midline signal did not change in response to amputation. White broken line indicates the plane of amputation. (C) Alternating $DiBAC_4(3)$ and $DiBAC_4(3)$-bright-field overlays of the tadpole; the bottom row of images show the right and left limbs of the same tadpole at 4x higher magnification before and after amputation. Scale bars: 500 μm. White outlines represent the boundaries of the limb, while the yellow lines represent the start and finish points of the signal seen on each limb, the measurements that taken as described in the Results. White broken line indicates the plane of amputation. 3C shows a overview (0.75x) of the tadpole, and the bottom row of images shows the right and left limbs of the same tadpole at 4x before and after amputation.
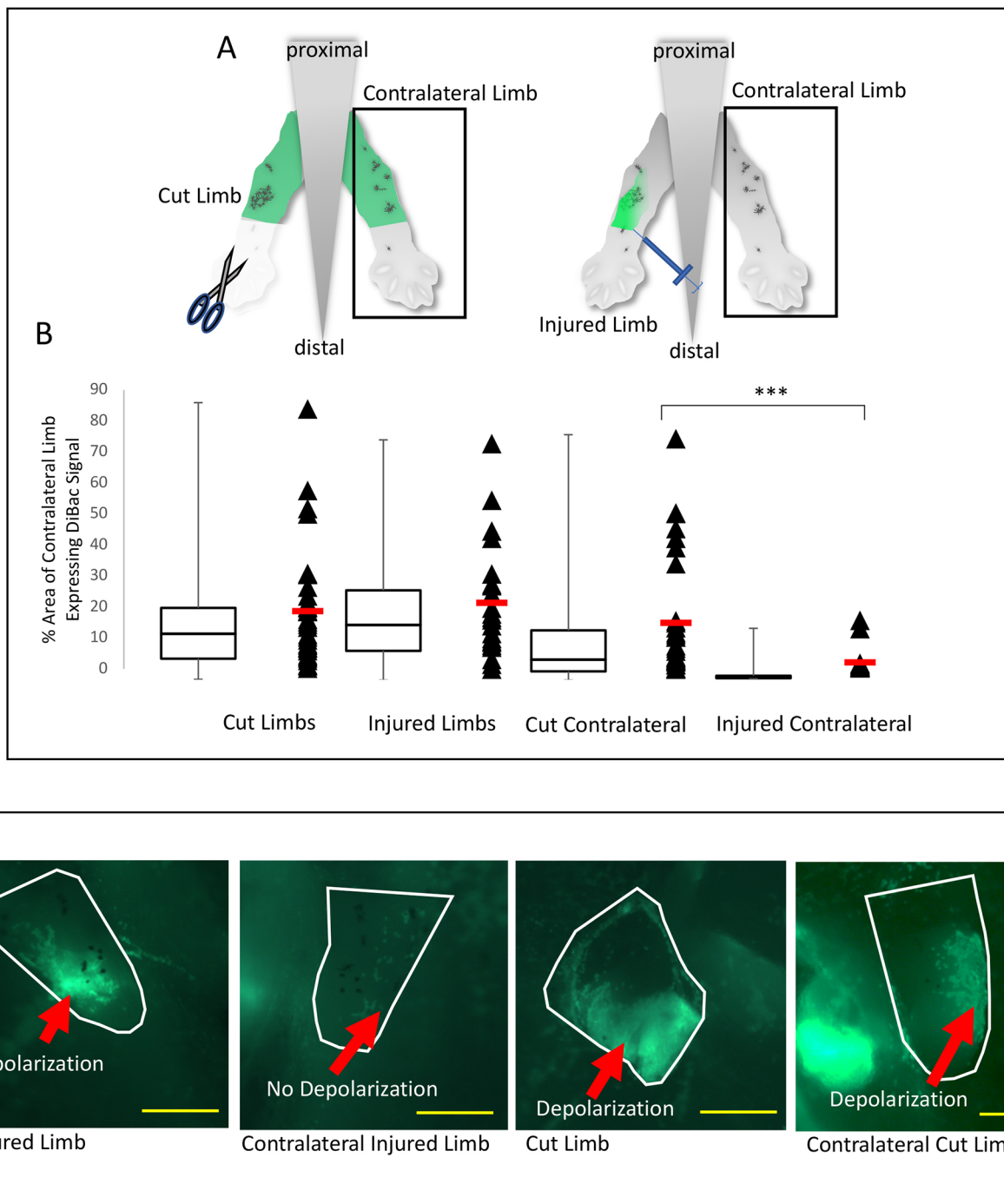
Fig. 4. Contralateral limbs respond to amputation, but not to injury. (A) Frogs were either fully amputated or injured with a syringe needle and the effects on the contralateral limbs were observed. (B,C) Quantification of results (B) and fluorescent imaging of amputated and injured limbs and contralateral limbs [DiBAC4(3) staining] (C). The box and whisker plot represents the data to the right of it in a different form. The red horizontal lines are the means of each dataset. The cut and injured limb treatments yielded no significant difference in response on the affected side. However, the contralateral limbs of injured animals exhibited significantly less depolarization than the contralateral limbs of amputated animals (Kruskal–Wallis test; injured, $n=32$; amputated, $n=23$; ***$P<0.0001$). The experiment was replicated three times. White outlines indicate the boundaries of the limb. Scale bars: 500 µm.

of limbs (Caine and McLaughlin, 2013; Tseng, 2017). None of the 21 unilateral kidney removals demonstrated an effect on the contralateral structure. Likewise, none of the 18 single eye removals demonstrated any response in the opposing eye (Fig. 5A,B). These data suggest that, at early stages, cross-body communication of limb injury information does not occur in all paired organs.

BIM is not mediated by a direct spinal cord path

One plausible hypothesis about cross-body injury information transfer concerns passage through the central nervous system (CNS), and in particular the spinal cord. To investigate the tissue mechanisms underlying BIM we interrupted the path that the amputation signal would take if it traveled through the spinal cord. Froglet extendor and flexor motor neuron leg extensions protrude
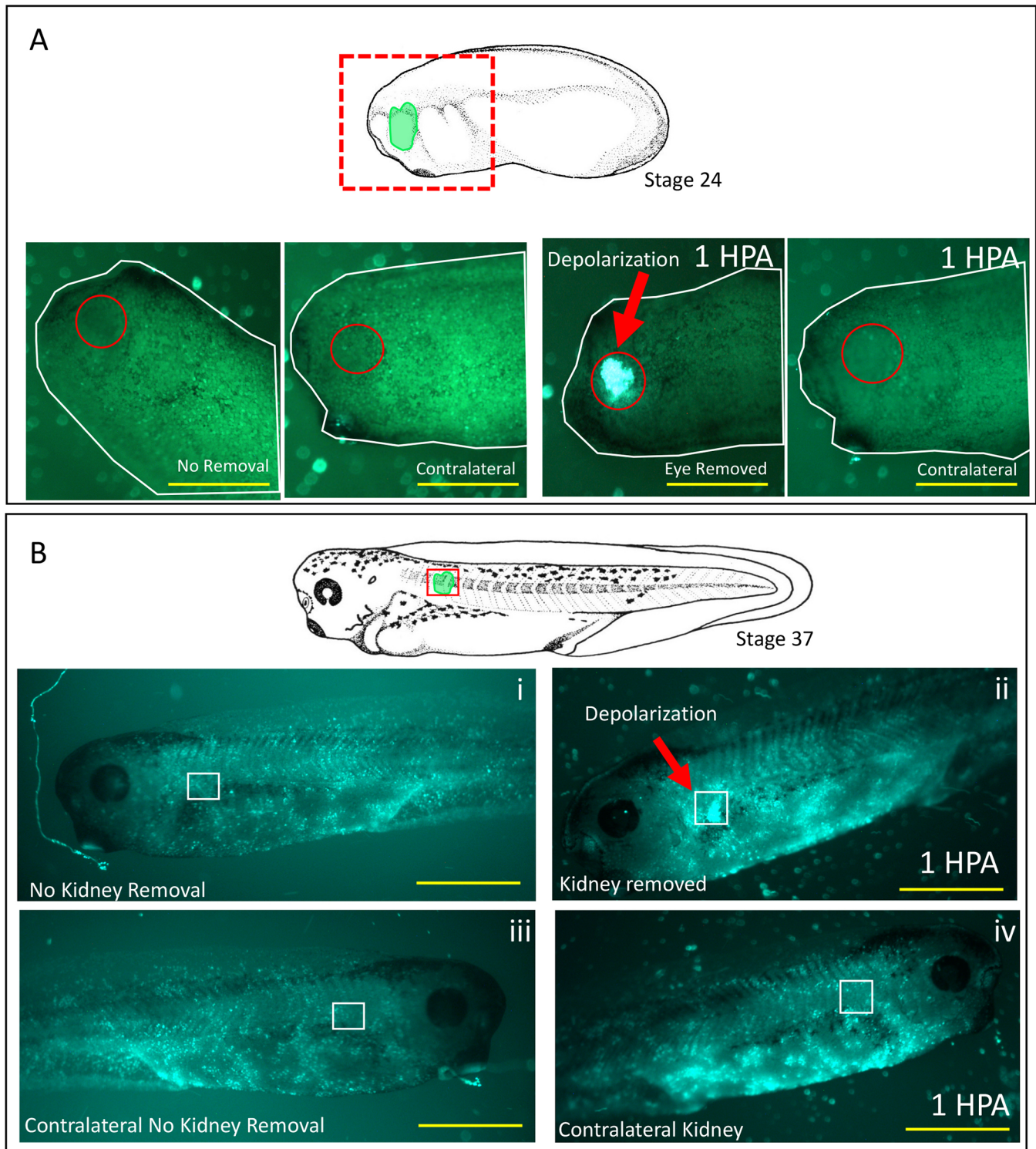
Fig. 5. Contralateral response does not occur in other paired structures. (A,B) Schematic and fluorescent imaging of stage 24 embryos that had one eye removed (A) and stage 37 embryos that had one kidney removed (B) [DiBAC4(3) staining]. The removal site of all eye-removal embryos showed depolarization, but no effect was observed in any of the contralateral eyes (*n*=18) (A). In kidney-removal embryos, all kidney removal sites showed depolarization after removal, but no effect was observed in any of the contralateral kidneys (*n*=21) (B). The experiment was performed once. Green shaded areas in schematics indicate the sites of organ removal and Dibac signal. Red box in A indicates the image field in the corresponding data images. Red circles indicate site of the eye. Red box in B corresponds to the area encompassed by the white boxes in the corresponding data images. White boxes show the site of the kidney. Scale bars: 500 μm.

from the eighth tail segment (Combes et al., 2004). For this reason, we transected the spinal cord at this eighth tail segment point, and split it open with forceps so that the 6-8 tail segments were disrupted

(Fig. 6A-B). Froglets undergoing only spinal cord transections did not differ significantly in the level of signal seen on either limb from control (uncut) animals. However, froglets that underwent
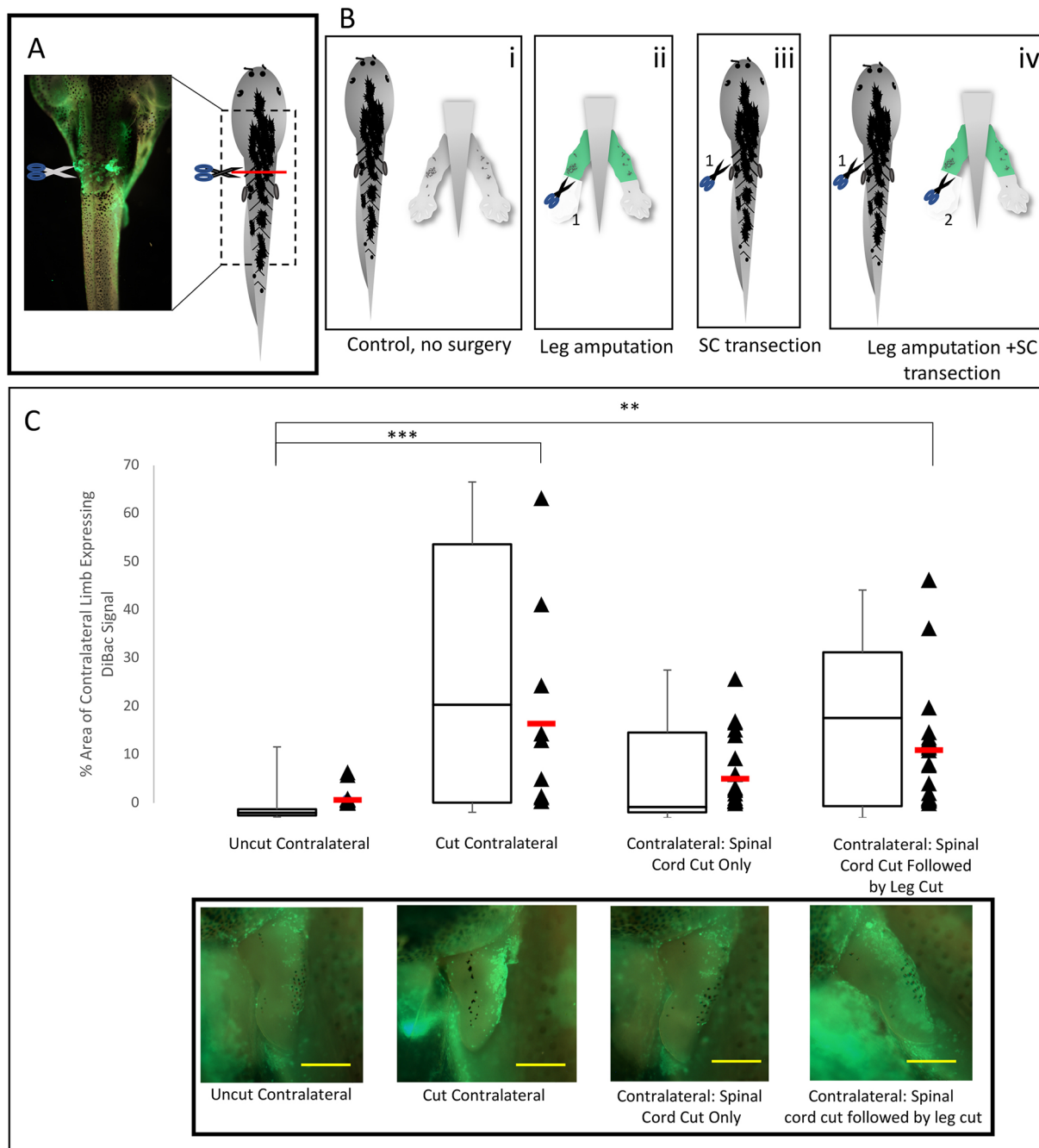
Fig. 6. BIM still occurs after spinal cord transection. (A) Fluorescent image and schematic showing the spinal cord transection at tail segments 6-8, severing connections to the extender and flexor motor neuron leg extensions. (B) Schematic showing experimental design: froglets were subject to leg amputation only, spine transection only or a spine transection followed by leg amputation. Controls underwent no surgery. (C) Quantification (top panel) and fluorescent imaging (bottom panel) of DiBAC$_4$(3) signal. Froglets showed no significant difference in DiBAC$_4$(3) signal between experiments in which the spine was transected before amputation, versus those in which spinal cords remained intact at the time of amputation (Kruskal–Wallis Test; amputated only, n=13; spinal cord transection and amputation, n=27). Froglets that underwent transection but no amputation showed no significant difference in DiBAC$_4$(3) signal from control froglets that did not undergo any surgery whatsoever (Kruskal–Wallis test; transection only, n=27; no surgery, n=14). The experiment was replicated four times. **P<0.001, ***P<0.0001. The box and whisker plot represents the data to the right of it in a different form. The red horizontal lines are the means of each dataset. White outline indicates boundaries of the limb. Scale bars: 500 µm.

transections alone also exhibited a degree of BIM signal, indicating that spinal cord damage may also elicit a modest response in the distant regions of the hindlimb surface. To determine whether the response to spinal cord transection elicited the same mirroring response as amputation of the limb, extension of the DiBAC$_4$(3) signal on froglet limbs undergoing spinal cord transections only was analyzed in a regression analysis. The correlation between the

length of the DiBAC$_4$(3) signal down the limb and the length down the opposing limb was measured, and no significant correlation was found (r=0.21, P=0.38, Fig. S3C).

Crucially, spinal cord transection immediately before leg amputation did not reduce the BIM signal seen on the contralateral limb compared with that seen in froglets that underwent only limb amputations and had an intact spinal cord

(Fig. 6C). Thus, we conclude that additional pathways exist and a spinal cord path is not required for BIM long-range injury signaling.

DISCUSSION

Here, we characterize the bioelectric state of the contralateral leg after injury. Functional roles of bioelectric states in the cut limb are being investigated elsewhere (Golding et al., 2016).

Information on injury is available at long distance *in vivo*

We have characterized BIM as a unique physiological phenomenon: a cross-body mirrored bioelectric signal in the skin of contralateral hindlimbs of regenerating *Xenopus laevis* froglets in response to one hindlimb amputation. It should be noted that the observed signal may be under-reporting the magnitude of the *in vivo* physiological response, because all of the surgeries had to be done in the presence of the voltage-gated sodium channel (NaV) blocker anesthetic tricaine, for reasons of animal welfare. It is also possible that NaVs are not involved in BIM, as we observed robust contralateral injury-induced response despite complete tricaine-induced anesthesia.

The quantitatively predictive aspect of the contralateral signal for different locations and types of damage (Figs 3 and 4) rules out a number of alternative hypotheses about the source of dye signal in the undamaged leg. Specifically, the signal pattern's dependence on the specific type and location of damage in the distant limb reveals that it is reporting the active physiological state of the body and not an artifact of generic local dye dynamics on the limb being imaged. Furthermore, the intensity of the signal can be predictively manipulated with increased K^+ and Cl^- ion concentrations and does not manifest when the limbs are stained with a dye that is not sensitive to membrane voltage, revealing that the signal is a function of ion concentrations in the undamaged leg. Thus, we believe that an important aspect of cross-body damage response is bioelectrical. However, a few caveats must be noted.

Although $DiBAC_4(3)$ is a powerful and widely used tool for detecting membrane depolarization, it is not a direct or quantitative measure of V_{mem}. Although $DiBAC_4(3)$ reveals a clear physiological response to contralateral damage, voltage change is only one of the several inputs that could be revealed by this signal. We conducted several control experiments to verify that $DiBAC_4(3)$ responds to V_{mem} changes in our system (Fig. S1), but we cannot definitively say that the $DiBAC_4(3)$ fluorescent changes induced by amputation result only from membrane depolarization. It is formally possible that long-distance damage is inducing increased endocytosis ($DiBAC_4(3)$ internalization) in the skin of an undamaged limb; however, we did not observe any specific signal using the V_{mem}-insensitive dye Acridine Orange (Fig. S2D), and thus any such BIM-related dye endocytosis would have to be specific for $DiBAC_4(3)$ and not general.

Interestingly, we did observe evidence of increased apoptosis in contralateral limbs (Fig. S4A); a degree of programmed cell death in undamaged tissue may be an aspect of the BIM phenomenon. Its adaptive function, if any, is as yet unknown, but apoptosis is now known to be functionally important in regeneration of both amphibian and invertebrate models (Chera et al., 2009; Tseng et al., 2007). Unfortunately, because of technical limitations it is not practical to combine $DiBAC_4(3)$ staining (which must be done in the living state) with immunohistochemistry to determine at a cellular level how closely this apoptosis pattern matches with the BIM signal, nor is it known yet whether the induced apoptosis is a cause or an effect of the apparent membrane depolarization evident in our $DiBAC_4(3)$ stains (Boutillier et al., 1999; Franco et al., 2006;

Gilbert and Knox, 1997). The $DiBAC_4(3)$ staining patterns and those of the cleaved caspase 3 (CC3) marker for apoptotic cells are not identical. It is likely that $DiBAC_4(3)$ could be revealing some depolarized live cells, but also some apoptotic cells that are depolarized because of the dissipation of electrochemical gradient at death (Fig. S4A,B). Importantly, however, apoptotic depolarization is a bona fide bioelectric phenomenon, and is therefore consistent with our conclusion about the bioelectric signature of long-range damage. We are currently working to translate genetically encoded voltage sensing tools (Knopfel et al., 2015; Matzke and Matzke, 2015) into the *Xenopus* model system; such transgenic animals will eventually enable a more highly resolved understanding of the mechanistic basis of BIM.

This signal occurs in response to amputation, but not other types of injury, revealing that the BIM signal includes information about the nature of the injury. Furthermore, the plane of amputation correlates highly with the area of signal on the contralateral limb; the contralateral depolarization reveals that the uninjured leg not only detected that amputation occurred, but also gained additional information about its location. Interestingly, ~20% of the specimens did not exhibit signal on the contralateral limb. We have seen that signal on the contralateral limb decreases as froglets enter the refractory period (data not shown); thus, one possibility is that a few of the froglets used for this work were pre-refractory by anatomical staging (stages 50-53) but may have already entered the refractory, non-regenerative period. This variability may have important implications for biomedicine, as incomplete penetrance of phenotypes and side effects are still poorly understood. The mechanism underlying differential physiological responses and the variability in propagation of bioelectrical signals *in vivo* remain an active area of research (Durant et al., 2017). There did not appear to be any changes in these other regions in response to amputation. The significance of these other aspects of endogenous bioelectric gradients is not known, but their existence is fully consistent with a widespread role of voltage gradients in numerous aspects of physiology aside from injury response (Bates, 2015; McLaughlin and Levin, 2018).

Though BIM has not been studied in molecularly tractable model systems before, one classic phenomenon observed in deer may be relevant (Lobo et al., 2014). Amputation and other forms of injury to antlers or limbs have resulted in contralateral effects, namely, altered morphology of the unaffected antlers during regrowth in the season following the injury (Bubenik and Pavlansky, 1965). Some of these studies have implicated innervation in antler growth and patterning, showing that damage or lack of nerves in antlers results in improper growth the following year (Bubenik and Pavlansky, 1965; Bubenik, 1990; Marburger et al., 1972). Importantly, the degree of injury plays a functional role in the outcome of the morphology of the contralateral antler, suggesting that contralateral signals such as those we describe here can be functionally important in large, adult mammals.

Potential propagation mechanisms

The precise mechanism by which BIM transfers information across the body from the injured leg to the contralateral is not yet known. Future work will test candidate mechanisms including blood-mediated systemic factors (Rodgers et al., 2017), non-neural bioelectric patterns (Levin et al., 2017), brain-dependent signaling (Herrera-Rincon et al., 2017) etc. However, the speed with which this process occurs rules out classic cellular signaling mechanisms. Several canonical signaling pathways, such as Wnt, BMP, FGF, Shh and serotonin, have been implicated in regeneration and linked to

bioelectric signaling (Borodinsky and Belgacem, 2016; Pai et al., 2016; Tseng and Levin, 2013). However, each of these pathways functions via the comparatively slow diffusion of signaling molecules (Beck et al., 2006; Cannata et al., 2001; Endo et al., 1997; Nacu et al., 2016; Yokoyama et al., 2007), which is not compatible with the rapid onset of bioelectric signals we observed in the contralateral leg. Froglets at these stages have fully functioning circulatory systems, potentially allowing for delivery of a blood-borne factor within the timeframe that we observe.

The nervous system was an especially appealing candidate for the conduit for BIM information transfer, as it is optimized to rapidly transfer spatial information throughout the body. We found that the mechanism of signal transduction is likely not a direct path through the spinal cord, as spinal cord integrity is not required for the BIM signal to appear (Fig. 6). Interestingly, we found that embryos that underwent spinal cord transection alone did exhibit a BIM-like signal. We are in the process of developing sophisticated machine-learning based analyses of dye signal to extract signatures for specific types and regions of damage; a limitation of our current comparative area-based metric (and of the non-high-throughput *Xenopus* leg amputation assay) is that the spinal cord-induced signal is statistically similar to some leg amputation-induced signals. Importantly, however, the BIM signal is not a generic indicator of general body damage because it does not respond to eye damage (Fig. 5) and quantitatively reflects the position of damage in the leg (Figs 3 and 4). Moreover, we performed a regression analysis on the $DiBAC_4(3)$ staining patterns observed in froglets with transected spinal cords and found that there was no correlation between the length that the staining extended down one limb and the plane of amputation. Thus, although spinal cord damage elicits an observable fluorescent signal, it does not carry the same information as does the amputated limb (Fig. S3C).

Despite a lack of evidence for the requirement of the spinal cord in BIM, a large body of classical and modern work reveals that the CNS is important in regulating regenerative events (Farkas and Monaghan, 2017; Kumar and Brockes, 2012; Singer, 1952, 1965). For example, the nerve-dependent signaling pathway initiated by NRG1 signaling has been shown to prevent formation of a wound blastema and subsequently lead to failed regeneration in axolotl (Farkas et al., 2016). Finally, the brain has been shown to be necessary for normal nerve and muscle patterning in *Xenopus*, and normal innervation is necessary for successful regeneration (Herrera-Rincon et al., 2017; Singer, 1952). Future stimulation and blocking experiments targeting neural components in different regions of the body will independently test for the role of brain and peripheral innervation in the BIM process.

Potential uses and implications of BIM

One of the implications of this work is that contralateral limbs are not 'naïve' when an injury occurs. Thus, the common practice of using contralateral limbs as controls is potentially fraught with the potential for artifacts, as the side that is not operated on is not equivalent to a limb from an uninjured animal. This also raises the issue of the function of the contralateral depolarization. It should be noted that the contralateral signal preferentially manifests in froglets of regenerative stages, pointing to a possible regenerative function. It is not yet known whether this event is required for some aspect of regenerative response, and treating the contralateral limb with V_{mem}-altering strategies will be tested in subsequent functional work using transgenic *Xenopus* animals not yet available. There is a growing collection of work showing altered activity that is either systemic or specific to the contralateral limb in response to

amputation, including chondrocyte activation and IGF signaling to other tissues for 'catch-up growth', as well as cell cycle activation (Roselló-Díez et al., 2018; Johnson et al., 2017). This work, in combination with our present findings, points to a more generalized phenomenon that may also exist in mammalian systems.

Previous work in embryonic (Adams et al., 2016; Levin and Martyniuk, 2017; Pai et al., 2018), tumor (Chernet and Levin, 2013, 2014) and regenerative (Adams et al., 2007; Durant et al., 2017; Tseng et al., 2010) models has revealed bioelectric prepatterns that are not only correlates of growth and form but also functionally instructive. Thus, the existence of BIM suggests several avenues for biomedical application, including surrogate-site diagnostics such as those that are being developed for cancer field detection (Chernet et al., 2015; Chernet and Levin, 2013, 2014). It may be possible to gain actionable intelligence about injury processes in difficult-to-reach sites of the body by tracking bioelectric properties in other regions.

Future work will focus on several main areas of investigation, in addition to the aforementioned tests for the mechanism of propagation and for functional roles of the contralateral V_{mem} state. First, panels of physiological reporters and computational analysis (mutual information and similar metrics) can be used to extract the full information content from the physiological state of contralateral limbs. It may be possible to develop techniques to deeply understand the pathophysiological state of inaccessible organs through the V_{mem} and other metrics (pH, mitochondrial potentials, etc.) of their respective mapped sites. Real-time non-invasive imaging of the physiological state (Adams and Levin, 2012a) is a powerful modality for exploration in this context, and it is possible that the full encoding of the contralateral signal is evident in additional parameters besides resting potential. A related issue is the development of technology for probing beyond the skin. Optical reporters only allow access to the top layers of tissue; although the ectodermal layers are known to drive a lot of the important bioelectric dynamics (Robinson and Messerli, 1996), it is entirely possible that the ionic state of deep tissues bears useful information as well, and developing tools to access the deep tissue physiological state is a priority for future research.

Also, it is important to explore other pairs of organs to determine whether any exhibit this phenomenon. Adult animals must be examined for the ability of kidneys, lungs, eyes, brain hemispheres, forelimbs and other paired organs to communicate a damaged state contralaterally. Finally, although recent work in human cells *in vitro* (Li et al., 2016; Pai et al., 2016; Sundelacruz et al., 2008, 2013) and characterization of channelopathies (Kamate and Chetal, 2011; Kortum et al., 2015; Masotti et al., 2015; Veale et al., 2014; Xie et al., 2010) have confirmed the conservation of bioelectric signaling to mammals, BIM should be sought in mammalian models to determine the degree of evolutionary conservation of this system and bring it closer to biomedical use (Leppik et al., 2015).

Even if the signal is purely descriptive, surrogate site imaging could be a useful diagnostic tool; as far back as the 1930s, Burr reported the ability to detect tumors in rabbits based on distant bioelectric measurements (Burr, 1940; Burr et al., 1938). However, if the contralateral depolarization region is functional and is part of a bi-directional communication system with the injury site, then delivering optogenetically or pharmacologically induced stimulation to depolarize cells in surrogate sites could circumvent the problem of surgery in more inaccessible structures. Further characterization and investigation of BIM may one day provide the ability to perform surrogate site intervention, setting the appropriate physiological state in one region of the body to affect pathology

elsewhere. The understanding and control of such whole-body communication systems represent a key challenge for systems-level integrative medicine of the future (Levin, 2011).

MATERIALS AND METHODS
Animal husbandry
All experimental procedures using animals were approved by the Institutional Animal Care and Use Committee (IACUC) and Tufts University Department of Laboratory Animal Medicine (DLAM) under protocol number M2017-53. *Xenopus laevis* froglets were ordered weekly from Nasco in batches of ~25 and allowed to acclimate at 22°C for seven days before amputation. Once acclimated, froglets were anesthetized with a 250 ml solution of 0.005% tricaine methanesulfonate (MS222) (Synde) and $0.1\times$ Marc's modified Ringer's (MMR) (made in-house) and amputated. After amputation, froglets were allowed to recover in the prepared 1:1000 dissolved $DiBAC_4(3)$ (Thermo Fisher Scientific) solution for 1 HPA (after the final amputation on the final tadpole was made). Once recovered, and after the 1 h had passed, froglets were again anesthetized with MS222 for imaging. Following imaging, froglets were returned to tanks with frog water and stored at room temperature until the 24 and 48 h imaging time points, at which time they were again anesthetized with MS222 and immersed in $DiBAC_4(3)$. After all imaging was complete, the froglets were returned to their tanks to be stored and cared for. They were fed and their tanks were cleaned and given new frog water three times per week.

Amputation, injury and spinal cord transection
Froglets were amputated after immersion in 0.005% MS222 in $0.1\times$ MMR for ~10 min, until completely unresponsive to stimuli. Using a dissecting microscope for guidance, the right hindleg of each tadpole was amputated at the tibiofibular region using surgical scissors. Froglets that were injured were punctured with a sterile 22G 0.7 mm syringe needle (Thermo Fisher Scientific) through the tibiofibular region of the limb. Froglets undergoing spinal cord transection were cut using surgical scissors, severing tail segments 6-8, the position of the extender and flexor motor neuron leg extensions (Combes et al., 2004). Control froglets were subject to the same conditions, but without amputation or injury following MS222 anesthesia. Experiments investigating other paired structures (developing eyes and kidneys) were initiated with MS222 exposure. Stage 24 and 37 embryos were used to perform eye and kidney removals, respectively, as the organs are regenerative at the respective stages. Following anesthetization, one eye of each stage 24 embryo or one kidney of each stage 37 embryo was removed using forceps. Treatment groups for each experiment were determined randomly, by taking the desired number of froglets for a given experiment at random from a tank and placing them in an assigned treatment container.

Imaging with DiBAC₄(3) and Acridine Orange
$DiBAC_4(3)$ was prepared in $0.1\times$ MMR according to protocol (Adams and Levin, 2012b) except that a final concentration of 10 µM was used. For Acridine Orange imaging, a 10 mM stock solution of Acridine Orange in dimethyl sulfoxide (DMSO) was diluted to a working concentration of 10 µM in $0.1\times$ MMR. Froglets were allowed to recover in this solution for 1 HPA before further addition of MS222 (0.005%) before imaging. At later time points (24 and 48 HPA) the solution was prepared again, with additional MS222 (0.005%), and froglets were allowed to soak for 30 min before imaging, to allow for sufficient dye permeation. Different treatment groups were imaged in tandem so that any increase in signal occurring due to longer incubation time occurred in all groups equally and would not affect the differences in the results of any of the treatments shown.

Treatment with depolarizing solution
Froglets were anesthetized by soaking in 250 ml 0.01% MS222 and $0.1\times$ MMR for 10 min. Pre-treatment, froglets were imaged with $DiBAC_4(3)$, then their hindlimbs were amputated. Immediately following amputation, froglets were placed in 90 mM potassium gluconate in $0.1\times$ MMR and allowed to soak for 45 min. Controls remained in $0.1\times$ MMR. Following salt treatment, froglets were imaged in their respective treatment media.

Immunohistochemistry
Immunohistochemistry was performed after fixing froglets in 1 part formaldehyde, 1 part MEMFA [100 mM MOPS (pH 7.4), 2 mM EGTA, 1 mM $MgSO_4$, 3.7% (v/v) formaldehyde] and 8 parts H_2O overnight at 4°C. Froglets were rinsed for 3×10 min in $0.1\times$ MMR before beginning the immunohistochemistry protocol. Froglets were incubated overnight with CC3 antibody (Cell Signaling Technology, 9661S, 1:300) in blocking solution (Roche, 11096176001). Secondary antibody incubation was performed for 90 min using 555 goat anti-rabbit secondary antibody and blocking solution, and froglets were imaged immediately after rinsing.

Imaging and image analysis
Images were taken using a Nikon SMZ1500 microscope with a Retiga 2000R camera and Retiga Q-Capture imaging software. Gain and exposure were kept consistent across all imaging sessions for all trials. Data acquired for the purpose of measuring image intensity was dark-field and flat-field corrected by taking dark- and flat-field images with the same settings used for data acquisition. Adobe Photoshop was used to crop (lasso tool) and invert images onto a white background so that only legs were present. They were then analyzed using the color threshold function on ImageJ, so that the same amount of signal area as could be seen with the naked eye on the average photo was detected. The threshold was applied to all photos in the series. The threshold was then changed to measure the entire area of the limb and again applied to the series, so that the ratio of the two (fluorescence/limb) could be used for determining any differences between groups or time points (Fig. S5). For some experiments, including potassium gluconate analysis, intensity rather than area was measured: limbs were traced and the 'average intensity' measurement tool on ImageJ was used to determine the intensity of fluorescence in the limbs. Two images were taken for each animal, one of the uncut contralateral leg and one of the cut limb. A stage was assigned to the tadpole featured in each set of two photos using the Xenbase online database of Xenopus development stages by comparing the contralateral leg with the images provided on the database (www.xenbase.com).

Statistics and analysis
Statistical analyses were performed using Prism v.5 (GraphPad Software). In order to compare across treatment groups and time points (injury and amputation, 0.5 HPA, 1 HPA, 24 HPA and 48 HPA time points), a Kruskal–Wallis test was used to analyze the values acquired from the ratio of the fluorescent area to the area of the entire limb (in both cut and contralateral legs). For statistics comparing two groups (i.e. control and amputated froglets, control animals and potassium gluconate-treated animals), post-hoc comparisons were performed using the Dunn's multiple comparisons test. Differences were considered significant at $P<0.01$. In order to analyze the correlation between information from cut and contralateral limbs, a linear regression analysis was performed in Microsoft Excel.

DEVELOPMENT

Supplementary information
Supplementary information available online at
http://dev.biologists.org/lookup/doi/10.1242/dev.164210.supplemental

References

Adams, D. S. and Levin, M. (2012a). General principles for measuring resting membrane potential and ion concentration using fluorescent bioelectricity reporters. *Cold Spring Harb. Protoc.* **2012**, 385-397.

Adams, D. S. and Levin, M. (2012b). Measuring resting membrane potential using the fluorescent voltage reporters DiBAC4(3) and CC2-DMPE. *Cold Spring Harb. Protoc.* **2012**, 459-464.

Adams, D. S., Masi, A. and Levin, M. (2007). H+ pump-dependent changes in membrane voltage are an early mechanism necessary and sufficient to induce Xenopus tail regeneration. *Development* **134**, 1323-1335.

Adams, D. S., Tseng, A.-S. and Levin, M. (2013). Light-activation of the Archaerhodopsin H(+)-pump reverses age-dependent loss of vertebrate regeneration: sparking system-level controls in vivo. *Biol. Open* **2**, 306-313.

Adams, D. S., Uzel, S. G., Akagi, J., Wlodkowic, D., Andreeva, V., Yelick, P. C., Devitt-Lee, A., Pare, J. F. and Levin, M. (2016). Bioelectric signalling via potassium channels: a mechanism for craniofacial dysmorphogenesis in KCNJ2-associated Andersen-Tawil Syndrome. *J. Physiol.* **594**, 3245-3270.

Bates, E. (2015). Ion channels in development and cancer. *Annu. Rev. Cell Dev. Biol.* **31**, 231-247.

Beane, W. S., Morokuma, J., Adams, D. S. and Levin, M. (2011). A Chemical genetics approach reveals H,K-ATPase-mediated membrane voltage is required for planarian head regeneration. *Chem. Biol.* **18**, 77-89.

Beane, W. S., Morokuma, J., Lemire, J. M. and Levin, M. (2013). Bioelectric signaling regulates head and organ size during planarian regeneration. *Development* **140**, 313-322.

Beck, C. W., Christen, B., Barker, D. and Slack, J. M. (2006). Temporal requirement for bone morphogenetic proteins in regeneration of the tail and limb of Xenopus tadpoles. *Mech. Dev.* **123**, 674-688.

Blackiston, D., Adams, D. S., Lemire, J. M., Lobikin, M. and Levin, M. (2011). Transmembrane potential of GlyCl-expressing instructor cells induces a neoplastic-like conversion of melanocytes via a serotonergic pathway. *Dis. Model. Mech.* **4**, 67-85.

Borgens, R. B. (1986). The role of natural and applied electric fields in neuronal regeneration and development. *Prog. Clin. Biol. Res.* **210**, 239-250.

Borgens, R. B., Vanable, J. W., Jr. and Jaffe, L. F. (1977a). Bioelectricity and regeneration: large currents leave the stumps of regenerating newt limbs. *Proc. Natl. Acad. Sci. USA* **74**, 4528-4532.

Borgens, R. B., Vanable, J. W., Jr. and Jaffe, L. F. (1977b). Bioelectricity and regeneration. I. Initiation of frog limb regeneration by minute currents. *J. Exp. Zool.* **200**, 403-416.

Borodinsky, L. N. and Belgacem, Y. H. (2016). Crosstalk among electrical activity, trophic factors and morphogenetic proteins in the regulation of neurotransmitter phenotype specification. *J. Chem. Neuroanat.* **73**, 3-8.

Borodinsky, L. N., Belgacem, Y. H. and Swapna, I. (2012). Electrical activity as a developmental regulator in the formation of spinal cord circuits. *Curr. Opin. Neurobiol.* **22**, 624-630.

Boutillier, A. L., Kienlen-Campard, P. and Loeffler, J. P. (1999). Depolarization regulates cyclin D1 degradation and neuronal apoptosis: a hypothesis about the role of the ubiquitin/proteasome signalling pathway. *Eur. J. Neurosci.* **11**, 441-448.

Bubenik, G. A. (1990). The role of the nervous system in the growth of antlers. In *Horns, Pronghorns, and Antlers: Evolution, Morphology, Physiology, and Social Significance* (ed. G. A. Bubenik and A. B. Bubenik), pp. 339-358. New York, NY: Springer New York.

Bubenik, A. B. and Pavlansky, R. (1965). Trophic responses to trauma in growing antlers. *J. Exp. Zool.* **159**, 289-302.

Burr, H. S. (1940). Biologic organization and the cancer problem. *Yale J. Biol. Med.* **12**, 277-282.

Burr, H. S., Strong, L. C. and Smith, G. M. (1938). Bioelectric correlates of methylcolantherene-induced tumors in mice. *Yale J. Biol. Med.* **10**, 539-544.

Caine, S. T. and McLaughlin, K. A. (2013). Regeneration of functional pronephric proximal tubules after partial nephrectomy in Xenopus laevis. *Dev. Dyn.* **242**, 219-229.

Cannata, S. M., Bagni, C., Bernardini, S., Christen, B. and Filoni, S. (2001). Nerve-independence of limb regeneration in larval Xenopus laevis is correlated to the level of fgf-2 mRNA expression in limb tissues. *Dev. Biol.* **231**, 436-446.

Chera, S., Ghila, L., Dobretz, K., Wenger, Y., Bauer, C., Buzgariu, W., Martinou, J. C. and Galliot, B. (2009). Apoptotic cells provide an unexpected source of Wnt3 signaling to drive hydra head regeneration. *Dev. Cell* **17**, 279-289.

Chernet, B. T. and Levin, M. (2013). Transmembrane voltage potential is an essential cellular parameter for the detection and control of tumor development in a Xenopus model. *Dis. Model. Mech.* **6**, 595-607.

Chernet, B. T. and Levin, M. (2014). Transmembrane voltage potential of somatic cells controls oncogene-mediated tumorigenesis at long-range. *Oncotarget* **5**, 3287-3306.

Chernet, B. T., Fields, C. and Levin, M. (2015). Long-range gap junctional signaling controls oncogene-mediated tumorigenesis in Xenopus laevis embryos. *Front. Physiol.* **5**, 519.

Combes, D., Merrywest, S. D., Simmers, J. and Sillar, K. T. (2004). Developmental segregation of spinal networks driving axial- and hindlimb-based locomotion in metamorphosing Xenopus laevis. *J. Physiol.* **559**, 17-24.

Dent, J. N. (1962). Limb regeneration in larvae and metamorphosing individuals of the South African clawed toad. *J. Morphol.* **110**, 61-77.

Durant, F., Morokuma, J., Fields, C., Williams, K., Adams, D. S. and Levin, M. (2017). Long-term, stochastic editing of regenerative anatomy via targeting endogenous bioelectric gradients. *Biophys. J.* **112**, 2231-2243.

Endo, T., Yokoyama, H., Tamura, K. and Ide, H. (1997). Shh expression in developing and regenerating limb buds of Xenopus laevis. *Dev. Dyn.* **209**, 227-232.

Farkas, J. E. and Monaghan, J. R. (2017). A brief history of the study of nerve dependent regeneration. *Neurogenesis* **4**, e1302216.

Farkas, J. E., Freitas, P. D., Bryant, D. M., Whited, J. L. and Monaghan, J. R. (2016). Neuregulin-1 signaling is essential for nerve-dependent axolotl limb regeneration. *Development* **143**, 2724-2731.

Franco, R., Bortner, C. D. and Cidlowski, J. A. (2006). Potential roles of electrogenic ion transport and plasma membrane depolarization in apoptosis. *J. Membr. Biol.* **209**, 43-58.

Frazee, O. E. (1909). The effect of electrical stimulation upon the rate of regeneration in Rana pipiens and Amblystoma jeffersonianum. *J. Exp. Zool.* **7**, 457-476.

Funk, R. H. W. (2013). Ion gradients in tissue and organ biology. *Biol. Syst.* **2**, 105.

Gilbert, M. and Knox, S. (1997). Influence of Bcl-2 overexpression on Na+/K(+)-ATPase pump activity: correlation with radiation-induced programmed cell death. *J. Cell. Physiol.* **171**, 299-304.

Golding, A., Guay, J. A., Herrera-Rincon, C., Levin, M. and Kaplan, D. L. (2016). A tunable silk hydrogel device for studying limb regeneration in adult xenopus laevis. *PLoS ONE* **11**, e0155618.

Herrera-Rincon, C., Pai, V. P., Moran, K. M., Lemire, J. M. and Levin, M. (2017). The brain is required for normal muscle and nerve patterning during early Xenopus development. *Nat. Commun.* **8**, 587.

Ivanov, V., Rezaeinejad, S. and Chu, J. (2013). Cell dualism: presence of cells with alternative membrane potentials in growing populations of bacteria and yeasts. *J. Bioenerg. Biomembr.* **45**, 505-510.

Jang, S. S., Park, J., Hur, S. W., Hong, Y. H., Hur, J., Chae, J. H., Kim, S. K., Kim, J., Kim, H. S. and Kim, S. J. (2011). Endothelial progenitor cells functionally express inward rectifier potassium channels. *Am. J. Physiol. Cell Physiol.* **301**, C150-C161.

Jia, X., Yang, J., Song, W., Li, P., Wang, X., Guan, C., Yang, L., Huang, Y., Gong, X., Liu, M. et al. (2013). Involvement of large conductance Ca(2+)-activated K (+) channel in laminar shear stress-induced inhibition of vascular smooth muscle cell proliferation. *Pflugers Arch.* **465**, 221-232.

Johnson, K., Bateman, J., DiTommaso, T., Wong, A. Y. and Whited, J. L. (2017). Systemic cell cycle activation is induced following complex tissue injury in axolotl. *Dev. Biol.* **433**, 461-472.

Kamate, M. and Chetal, V. (2011). Andersen Tawil syndrome-periodic paralysis with dysmorphism. *Indian Pediatr.* **48**, 64-65.

King, M. W., Neff, A. W. and Mescher, A. L. (2012). The developing xenopus limb as a model for studies on the balance between inflammation and regeneration. *Anat. Rec.*

Knopfel, T., Gallero-Salas, Y. and Song, C. (2015). Genetically encoded voltage indicators for large scale cortical imaging come of age. *Curr. Opin. Chem. Biol.* **27**, 75-83.

Kortum, F., Caputo, V., Bauer, C. K., Stella, L., Ciolfi, A., Alawi, M., Bocchinfuso, G., Flex, E., Paolacci, S., Dentici, M. L. et al. (2015). Mutations in KCNH1 and ATP6V1B2 cause Zimmermann-Laband syndrome. *Nat. Genet.* **47**, 661-667.

Krotz, F., Riexinger, T., Buerkle, M. A., Nithipatikom, K., Gloe, T., Sohn, H.-Y., Campbell, W. B. and Pohl, U. (2004). Membrane-potential-dependent inhibition of platelet adhesion to endothelial cells by epoxyeicosatrienoic acids. *Arterioscler. Thromb. Vasc. Biol.* **24**, 595-600.

Kumar, A. and Brockes, J. P. (2012). Nerve dependence in tissue, organ, and appendage regeneration. *Trends Neurosci.* **35**, 691-699.

Leppik, L. P., Froemel, D., Slavici, A., Ovadia, Z. N., Hudak, L., Henrich, D., Marzi, I. and Barker, J. H. (2015). Effects of electrical stimulation on rat limb regeneration, a new look at an old model. *Sci. Rep.* **5**, 18353.

Levin, M. (2007). Large-scale biophysics: ion flows and regeneration. *Trends Cell Biol.* **17**, 262-271.

Levin, M. (2011). The wisdom of the body: future techniques and approaches to morphogenetic fields in regenerative medicine, developmental biology and cancer. *Regen. Med.* **6**, 667-673.

Levin, M. (2014a). Endogenous bioelectrical networks store non-genetic patterning information during development and regeneration. *J. Physiol.* **592**, 2295-2305.

Levin, M. (2014b). Molecular bioelectricity: how endogenous voltage potentials control cell behavior and instruct pattern regulation in vivo. *Mol. Biol. Cell* **25**, 3835-3850.

Levin, M. and Martyniuk, C. J. (2017). The bioelectric code: an ancient computational medium for dynamic control of growth and form. *Biosystems* **164**, 76-93.

Levin, M. and Mercola, M. (1999). Gap junction-mediated transfer of left-right patterning signals in the early chick blastoderm is upstream of Shh asymmetry in the node. *Development* **126**, 4703-4714.

Levin, M., Thorlin, T., Robinson, K. R., Nogi, T. and Mercola, M. (2002). Asymmetries in H+/K+-ATPase and cell membrane potentials comprise a very early step in left-right patterning. *Cell* **111**, 77-89.

Levin, M., Pezzulo, G. and Finkelstein, J. M. (2017). Endogenous bioelectric signaling networks: exploiting voltage gradients for control of growth and form. *Annu. Rev. Biomed. Eng.* **19**, 353-387.

Li, C., Levin, M. and Kaplan, D. L. (2016). Bioelectric modulation of macrophage polarization. *Sci. Rep.* **6**, 21044.

Lin, G., Chen, Y. and Slack, J. M. W. (2013). Imparting regenerative capacity to limbs by progenitor cell transplantation. *Dev. Cell* **24**, 41-51.

Lobo, D., Solano, M., Bubenik, G. A. and Levin, M. (2014). A linear-encoding model explains the variability of the target morphology in regeneration. *J. R. Soc. Interface.* **11**, 20130918.

Marburger, R. G., Robinson, R. M., Thomas, J. W., Andregg, M. J. and Clark, K. A. (1972). Antler malformation produced by leg injury in white-tailed deer. *J. Wildl. Dis.* **8**, 311-314.

Masotti, A., Uva, P., Davis-Keppen, L., Basel-Vanagaite, L., Cohen, L., Pisaneschi, E., Celluzzi, A., Bencivenga, P., Fang, M., Tian, M. et al. (2015). Keppen-lubinsky syndrome is caused by mutations in the inwardly rectifying K(+) Channel Encoded by KCNJ6. *Am. J. Hum. Genet.* **96**, 295-300.

Matzke, A. J. and Matzke, M. (2015). Expression and testing in plants of ArcLight, a genetically-encoded voltage indicator used in neuroscience research. *BMC Plant Biol.* **15**, 245.

McCaig, C. D., Rajnicek, A. M., Song, B. and Zhao, M. (2005). Controlling cell behavior electrically: current views and future potential. *Physiol. Rev.* **85**, 943-978.

McLaughlin, K. A. and Levin, M. (2018). Bioelectric signaling in regeneration: Mechanisms of ionic controls of growth and form. *Dev. Biol.* **433**, 177-189.

Morgan, T. H. and Dimon, A. C. (1904). An examination of the problem of physiological 'polarity' and electrical polarity in the earthworm. *J. Exp. Zool.* **1**, 331-347.

Nacu, E., Gromberg, E., Oliveira, C. R., Drechsel, D. and Tanaka, E. M. (2016). FGF8 and SHH substitute for anterior-posterior tissue interactions to induce limb regeneration. *Nature* **533**, 407-410.

Neff, A. W., King, M. W. and Mescher, A. L. (2011). Dedifferentiation and the role of sall4 in reprogramming and patterning during amphibian limb regeneration. *Dev. Dyn.* **240**, 979-989.

Nieuwkoop, P. D. and Faber, J. (1967). *Normal Table of Xenopus laevis (Daudin).* Amsterdam: North-Holland.

Oviedo, N. J., Nicolas, C. L., Adams, D. S. and Levin, M. (2008). Live imaging of planarian membrane potential using DiBAC4(3). *Cold Spring Harb. Protoc.* **2008**, pdb.prot5055.

Pai, V. P., Aw, S., Shomrat, T., Lemire, J. M. and Levin, M. (2012). Transmembrane voltage potential controls embryonic eye patterning in Xenopus laevis. *Development* **139**, 313-323.

Pai, V. P., Lemire, J. M., Chen, Y., Lin, G. and Levin, M. (2015a). Local and long-range endogenous resting potential gradients antagonistically regulate apoptosis and proliferation in the embryonic CNS. *Int. J. Dev. Biol.* **59**, 327-340.

Pai, V. P., Lemire, J. M., Pare, J. F., Lin, G., Chen, Y. and Levin, M. (2015b). Endogenous gradients of resting potential instructively pattern embryonic neural tissue via notch signaling and regulation of proliferation. *J. Neurosci.* **35**, 4366-4385.

Pai, V. P., Martyniuk, C. J., Echeverri, K., Sundelacruz, S., Kaplan, D. L. and Levin, M. (2016). Genome-wide analysis reveals conserved transcriptional responses downstream of resting potential change in Xenopus embryos, axolotl regeneration, and human mesenchymal cell differentiation. *Regeneration (Oxf)* **3**, 3-25.

Pai, V. P., Pietak, A., Willocq, V., Ye, B., Shi, N. Q. and Levin, M. (2018). HCN2 Rescues brain defects by enforcing endogenous voltage pre-patterns. *Nat. Commun.* **9**, 998.

Pare, J. F., Martyniuk, C. J. and Levin, M. (2017). Bioelectric regulation of innate immune system function in regenerating and intact Xenopus laevis. *Npj Regen. Med.* **2**, 15.

Perathoner, S., Daane, J. M., Henrion, U., Seebohm, G., Higdon, C. W., Johnson, S. L., Nüsslein-Volhard, C. and Harris, M. P. (2014). Bioelectric signaling regulates size in zebrafish fins. *PLoS Genet.* **10**, e1004080.

Poss, K. D. (2010). Advances in understanding tissue regenerative capacity and mechanisms in animals. *Nat. Rev. Genet.* **11**, 710-722.

Robinson, K. and Messerli, M. (1996). Electric embryos: the embryonic epithelium as a generator of developmental information. In *Nerve Growth and Guidance* (ed. C. McCaig), pp. 131-141. Portland: Portland Press.

Rodgers, J. T., Schroeder, M. D., Ma, C. and Rando, T. A. (2017). HGFA is an injury-regulated systemic factor that induces the transition of stem cells into GAlert. *Cell Rep* **19**, 479-486.

Rose, S. M. (1974). Bioelectric control of regeneration in tubularia. *Am. Zool.* **14**, 797-803.

Roselló-Díez, A., Madisen, L., Bastide, S., Zeng, H. and Joyner, A. L. (2018). Cell-nonautonomous local and systemic responses to cell arrest enable long-bone catch-up growth in developing mice. *PLoS Biol.* **16**, e2005086.

Sharma, K. K. and Niazi, I. A. (1990). Restoration of limb regeneration ability in frog tadpoles by electrical stimulation. *Indian J. Exp. Biol.* **28**, 733-738.

Singer, M. (1952). The influence of the nerve in regeneration of the amphibian extremity. *Q. Rev. Biol.* **27**, 169-200.

Singer, M. (1965). A theory of the trophic nervous control of amphibian limb regeneration, including a re-evaluation of quantitative nerve requirements. In *Regeneration in Animals and Related Problems* (ed. V. Kiortsis and H. A. L. Trampusch). Amsterdam: North Holland Publ. Co.

Slack, J. M. W., Beck, C. W., Gargioli, C. and Christen, B. (2004). Cellular and molecular mechanisms of regeneration in Xenopus. *Philos. Trans. R. Soc. Lond. B Biol. Sci.* **359**, 745-751.

Slack, J. M. W., Lin, G. and Chen, Y. (2008). The Xenopus tadpole: a new model for regeneration research. *Cell. Mol. Life Sci.* **65**, 54-63.

Smith, S. D. (1974). Effects of electrode placement on stimulation of adult frog limb regeneration. *Ann. NY Acad. Sci.* **238**, 500-507.

Sundelacruz, S., Levin, M. and Kaplan, D. L. (2008). Membrane potential controls adipogenic and osteogenic differentiation of mesenchymal stem cells. *PLoS ONE* **3**, e3737.

Sundelacruz, S., Levin, M. and Kaplan, D. L. (2009). Role of membrane potential in the regulation of cell proliferation and differentiation. *Stem Cell Rev. Rep.* **5**, 231-246.

Sundelacruz, S., Levin, M. and Kaplan, D. L. (2013). Depolarization alters phenotype, maintains plasticity of predifferentiated mesenchymal stem cells. *Tissue Eng. Part A* **19**, 1889-1908.

Swapna, I. and Borodinsky, L. N. (2012). Interplay between electrical activity and bone morphogenetic protein signaling regulates spinal neuron differentiation. *Proc. Natl. Acad. Sci. USA* **109**, 16336-16341.

Tanaka, E. M. (2016). The molecular and cellular choreography of appendage regeneration. *Cell* **165**, 1598-1608.

Tanaka, E. M. and Reddien, P. W. (2011). The cellular basis for animal regeneration. *Dev. Cell* **21**, 172-185.

Tseng, A.-S. (2017). Seeing the future: using Xenopus to understand eye regeneration. *Genesis* **55**, e23003.

Tseng, A.-S. and Levin, M. (2008). Tail regeneration in *Xenopus* laevis as a model for understanding tissue repair. *J. Dent. Res.* **87**, 806-816.

Tseng, A.-S. and Levin, M. (2013). Cracking the bioelectric code: probing endogenous ionic controls of pattern formation. *Commun. Integr. Biol.* **6**, 1-8.

Tseng, A.-S., Adams, D. S., Qiu, D., Koustubhan, P. and Levin, M. (2007). Apoptosis is required during early stages of tail regeneration in Xenopus laevis. *Dev. Biol.* **301**, 62-69.

Tseng, A.-S., Beane, W. S., Lemire, J. M., Masi, A. and Levin, M. (2010). Induction of vertebrate regeneration by a transient sodium current. *J. Neurosci.* **30**, 13192-13200.

Vandenberg, L. N., Morrie, R. D. and Adams, D. S. (2011). V-ATPase-dependent ectodermal voltage and pH regionalization are required for craniofacial morphogenesis. *Dev. Dyn.* **240**, 1889-1904.

Veale, E. L., Hassan, M., Walsh, Y., Al-Moubarak, E. and Mathie, A. (2014). Recovery of current through mutated TASK3 potassium channels underlying Birk Barel syndrome. *Mol. Pharmacol.* **85**, 397-407.

Wang, E. T. and Zhao, M. (2010). Regulation of tissue repair and regeneration by electric fields. *Chin. J. Traumatol.* **13**, 55-61.

Wolff, C., Fuks, B. and Chatelain, P. (2003). Comparative study of membrane potential-sensitive fluorescent probes and their use in ion channel screening assays. *J. Biomol. Screen.* **8**, 533-543.

Xie, G., Harrison, J., Clapcote, S. J., Huang, Y., Zhang, J.-Y., Wang, L.-Y. and Roder, J. C. (2010). A new Kv1.2 channelopathy underlying cerebellar ataxia. *J. Biol. Chem.* **285**, 32160-32173.

Yasuda, T. and Adams, D. S. (2010). Physiological roles of ion channels in adult neural stem cells and their progeny. *J. Neurochem.* **114**, 946-959.

Yokoyama, H., Ogino, H., Stoick-Cooper, C. L., Grainger, R. M. and Moon, R. T. (2007). Wnt/beta-catenin signaling has an essential role in the initiation of limb regeneration. *Dev. Biol.* **306**, 170-178.

Yokoyama, H., Maruoka, T., Aruga, A., Amano, T., Ohgo, S., Shiroishi, T. and Tamura, K. (2011a). Prx-1 expression in Xenopus laevis scarless skin-wound healing and its resemblance to epimorphic regeneration. *J. Invest. Dermatol.* **131**, 2477-2485.

Yokoyama, H., Maruoka, T., Ochi, H., Aruga, A., Ohgo, S., Ogino, H. and Tamura, K. (2011b). Different requirement for Wnt/beta-catenin signaling in limb regeneration of larval and adult Xenopus. *PLoS ONE* **6**, e21721.

DEVELOPMENT